Random Copolymers Based on 3-Hexylthiophene and Benzothiadiazole with Induced π-Conjugation Length and Enhanced Open-Circuit Voltage Property for Organic Photovoltaics

JANG-YONG LEE, MIN-HEE CHOI, HO-JUN SONG, DOO-KYUNG MOON

Department of Materials Chemistry and Engineering, Konkuk University, 1 Hwayang-dong, Gwangjin-gu, Seoul 143-701, Korea

Received 12 March 2010; accepted 3 August 2010
DOI: 10.1002/pola.24280
Published online 20 September 2010 in Wiley Online Library (wileyonlinelibrary.com).

ABSTRACT: A series of donor-acceptor low-bandgap conjugated polymers, that is, HThmBT (m = 3, 6, 9, 12, 15), composed of regioregular 3-hexylthiophene segments and 2,1,3-benzothiadiazole units, were synthesized through the Stille coupling polymerization to optimize the π-conjugation length of the polymer and the intramolecular charge transfer (ICT) effect in the polymer backbone. The polymers had relatively low optical bandgaps ranging from 1.6 to 1.72 eV. Among these polymers, HTh6BT exhibited the best device performance with a power conversion efficiency (PCE) of 1.6%. Moreover, despite being based on thiophene, HTh6BT exhibited a high-open circuit voltage (V_{OC}) of over 0.8 V because of its low high occupied molecular orbital (HOMO) energy level. These results provided an effective strategy for designing and synthesizing low-bandgap conjugated polymers with broad absorption ranges and well-balanced energy levels. © 2010 Wiley Periodicals, Inc. J Polym Sci Part A: Polym Chem 48: 4875–4883, 2010

KEYWORDS: charge transport; conjugated polymers; copolymerization

INTRODUCTION Semiconducting polymers have been developed for the past several decades because of their capacity in organic electronics, such as organic photovoltaics (OPVs),[1–8] organic thin film transistors (OTFTs), [9–11] organic light emitting diodes (OLEDs),[12–16] and so forth. Among these applications, OPVs have generated considerable scientific and technical interest because of their potential for the large area fabrication of low-cost integrated circuit elements for large area and the feasibility of the production using various methods, such as spin coating, ink-jet printing, and roll-to-roll through a solution process.[17–22]

Since the discovery of the ultrafast, photoinduced charge transfer from a conjugated polymer to fullerene, a variety of high-performance organic photovoltaic materials have been demonstrated.[23–25] Nevertheless, regioregular poly(3-hexylthiophene) (P3HT) has still been regarded as one of the most important organic semiconductor materials because of its good stacking and charge carrier transport properties. Yang and coworkers[26] developed solar cells with an efficiency of 4.4% by varying the annealing time, and Carroll and coworkers[27,28] obtained a PCE of 5.2% through the optimization of the acceptor molar ratio and the different annealing conditions. On account of its good photovoltaic properties, P3HT has been considered an important donor material in tandem structured organic photovoltaic devices to improve the photovoltaic efficiency.[29] Despite a remarkable photovoltaic efficiency of over 5%, the poor oxidative stability and the restricted solar spectrum absorption range of approximately 650 nm P3HT have been considered insuperable obstacles for its applicability in photovoltaic devices.[30] These drawbacks are related to the unoptimized energy levels in combination with a soluble fullerene derivative.[31] In particular, the HOMO level of P3HT restricts the open circuit voltage and the oxidative stability.

Recently, various polymer materials have been vigorously investigated to enhance the photovoltaic efficiency and the oxidative stability by reducing the bandgap and optimizing the HOMO and lowest unoccupied molecular orbital (LUMO) energy levels.[32–35] The following three methods can be used to lower the polymer bandgap and arrange the energy levels[1]: introducing an electron withdrawing functional groups[2]; increasing the effective π-conjugation length[3]; and using the charge transport properties by introducing a donor/acceptor (DA) conjugated system. Since the HOMO energy level is decreased with decrease of the LUMO energy level on introducing an electron withdrawing functional groups, the polymer bandgap cannot be efficiently decreased through the first method.[36] The second method reduces the oxidative stability of the polymer because the ionization potential (IP), which corresponds to the HOMO levels in vacuum, depends upon the effective π-conjugation length.[37–40] In contrast to the first and second methods, the last method is regarded as an effective method for synthesizing a low-bandgap polymer because of effective ICT effects that the high energy level for

Correspondence to: D.-K. Moon (E-mail: dkmoon@konkuk.ac.kr)
Journal of Polymer Science: Part A: Polymer Chemistry, Vol. 48, 4875–4883 (2010) © 2010 Wiley Periodicals, Inc.

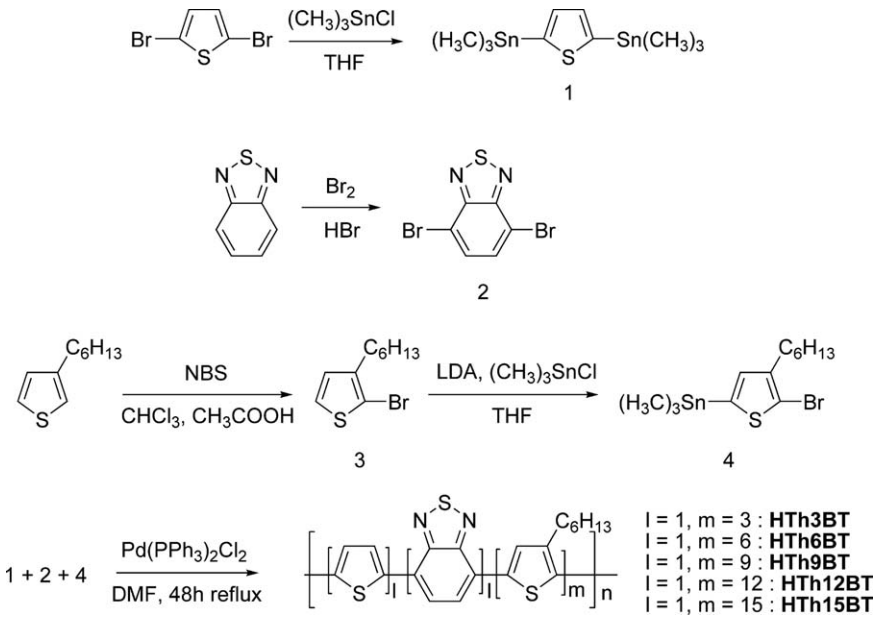

SCHEME 1 The synthetic routes of HThmBT series.

the HOMO of the donor and the low energy level for the LUMO of the acceptor results in a low-bandgap through the intrachain charge transfer from the donor to the acceptor.[41,42] Moreover, if the π-conjugation length of the polymer is efficiently reduced, the polymer can have oxidative stability and an increased V_{OC} value.

In this study, the low-bandgap polymers with well-balanced energy levels were developed by introducing a frequently used electron-deficient 2,1,3-benzothiadiazole unit into the poly(3-hexylthiophene) main chain to lower the bandgap and to control the number of thiophene rings in the oligothiophene segments, which improved the interchain packing, the solubility, and the effective ICT effects. A thiophene spacer was introduced into the polymer skeleton to control the orientation of the alkyl chains and to diminish the steric hindrance between the 3-hexylthiophene oligomer moiety and the electron withdrawing moiety. In polymerization, 2,5-bis(trimethyl stannyl)thiophene and 4,7-dibromo-2,1,3-benzothiadiazole were dissolved in solvent and stirred for 1 h under mild heating conditions so that the thiophene spacer neighbored with 2,1,3-benzothiadiazole, before 2-bromo-3-hexyl-5-trimethylstannylthiophene was added to the mixture.

New DA-type copolymers (HTh3BT to HTh15BT), based on 3-hexylthiophene and 2,1,3-benzothiadiazole, were synthesized through the Stille coupling reaction for the OPVs. During the synthesis, the molar ratio of 3-hexylthiophene was controlled to optimize the effective π-conjugation length of the 3-hexylthiophene oligomer. The bulk heterojunction-type devices were fabricated with 1-(3-methoxycarbonyl)propyl-1-phenyl-6,6-C-61 ($PC_{61}BM$) and 1-(3-methoxycarbonyl)propyl-1-phenyl-6,6-C-71 ($PC_{71}BM$) as the acceptors to investigate the photovoltaic properties. Despite the use of the thiophene-based DA-type copolymers, the devices with the polymers in the active layers displayed a high-open circuit voltage of 0.7–0.84 V. In particular, the device that used the HTh6BT/$PC_{71}BM$ blend film as the active layer exhibited a PCE value of 1.6% (V_{OC} = 0.82 V, J_{SC} = 5.5 mA/cm^2, FF = 0.35).

RESULTS AND DISCUSSION

Synthesis and Characterization

The synthesis process for the monomers and polymers is shown in Scheme 1. Monomers 1 and 2 were synthesized through a stannation of a 2,5-dibromothiophene and a bromination of a 2,1,3-benzothiadiazole, respectively. 3-Hexylthiophene was brominated with *N*-bromosuccsinimide (NBS) and then stannated with trimethyltinchloride to produce 4. HTh3BT to HTh15BT were synthesized through a Stille coupling reaction using $Pd(PPh_3)_2Cl_2$ as the catalyst in *N*,*N*′-dimethylformamide (DMF). Each polymer was well dissolved in common organic solvents, such as chloroform, THF, toluene, chlorobenzene (CB), and dichlorobenzene (DCB).

The molecular weight of the polymers was measured using the gel permeation chromatography (GPC) method, and polystyrene was used as the standard with THF as the eluent. The number average molecular weight (M_n) increased with increasing 3-hexylthiophene ratio in the polymer backbone because of the increased solubility of the polymers that was caused by the higher number of alkyl side chains in the polymer skeletons. The thermal properties of these copolymers were investigated using the thermogravimetric analysis (TGA) at a heating rate of 10 K/min (Fig. 1). All of the polymers had decomposition temperatures (T_d) near 420 °C, which indicated that these polymers exhibited good thermal stability, making them applicable for use in polymer solar cells and other optoelectronic devices. The results of molecular weight measurements and thermal properties are shown in Table 1.

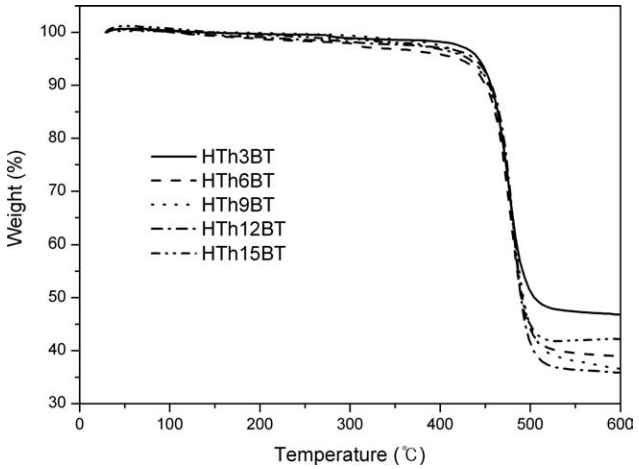

FIGURE 1 TGA curves of polymers.

Optical Properties

Figures 2 and 3 show the UV–vis absorption and the PL spectrum of HTh3BT to HTh15BT in the chloroform solution and the thin solid films, respectively. HTh3BT and HTh6BT exhibited maximum UV–vis absorption peaks (λ_{max}) at 387/553 nm and 408/536 nm, respectively, in solution. The λ_{max} of HTh9BT, HTh12BT, and HTh15BT were observed at 414/521, 426, and 428 nm, respectively. In Figure 2, the maximum UV–vis absorption peaks in the range of the long wavelength were lower than in the range of the short wavelength with increasing 3-hexylthiophene ratio. The UV–vis absorption spectra of HTh15BT was similar to P3HT, indicating that the polymer had similar photon absorption properties to P3HT at higher molar ratios of 3-hexylthiophene in the polymer backbone. HTh15BT exhibited high photon absorption properties below 500 nm, whereas the photon absorption properties in the long wavelength range over 500 nm were lower than the other polymer. HTh3BT and HTh6BT exhibited high absorption properties in the long wavelength range above 500 nm compared to HTh15BT. Considering that most of the photons were in the range from 500 to 900 nm in the solar spectrum, the photocurrent density and the incident photon-to-current conversion efficiency (IPCE) of HTh3BT and HTh6BT were expected to be better than the other polymers. The UV–vis absorption spectrum in the films indicated

TABLE 1 Molecular Weights of Synthesized Polymers

Polymer	BT:3-Hexylthiophene Molar Ratio	Yield (%)	M_n	M_w	M_w/M_n
HTh3BT	1:3	84	5,486	6,909	1.25
HTh6BT	1:6	84	11,684	22,855	1.95
HTh9BT	1:9	87	13,545	22,982	1.48
HTh12BT	1:12	94	20,840	66,488	3.1
HTh15BT	1:15	98	21,174	46,695	2.2

Molecular weights and polydispersity indexes determined by GPC in THF on the basis of polystyrene calibration.

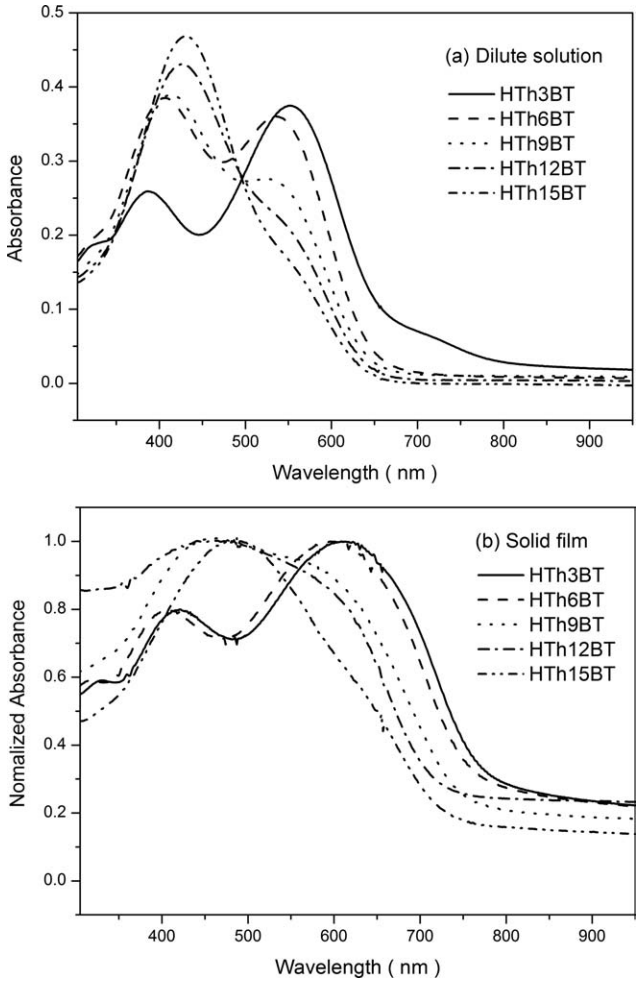

FIGURE 2 Comparison of UV−vis absorption spectra of polymers (a) in a solution (in chloroform at a concentration of 1 mg/mL), and (b) in a film.

similar tendencies to the solutions. The optical bandgap was calculated from the band edge of the UV–vis absorption spectrum in the film. The polymers had a relatively low optical bandgap of 1.6–1.72 eV. Among these polymers, HTh3BT, which had the lowest molar ratio of 3-hexylthiophene of the five polymers, exhibited the lowest bandgap. HTh3BT could effectively develop a molecular orbital overlap between 3-hexylthiophenes and 2,1,3-benzothiadiazole because of the ICT effect.[31] The absorption maxima of HTh6BT was similar to HTh3BT. However, HTh6BT could be more effective as the active layer material for the OPVs because it had a larger absorption area than HTh3BT.

The PL spectra of the polymers are displayed in Figure 3. In the solution, the five polymers had maximum emission peaks near 685 nm. However, strong emission property was appeared with increasing 3-hexylthiophene molar ratio near 570 nm for HTh9BT to HTh15BT. It may come from the oligo-thiophene's emission, whereas the longer wavelength peak is due to the benzothiadiazole's emission via energy transfer. The solid-state photoluminescence was observed in

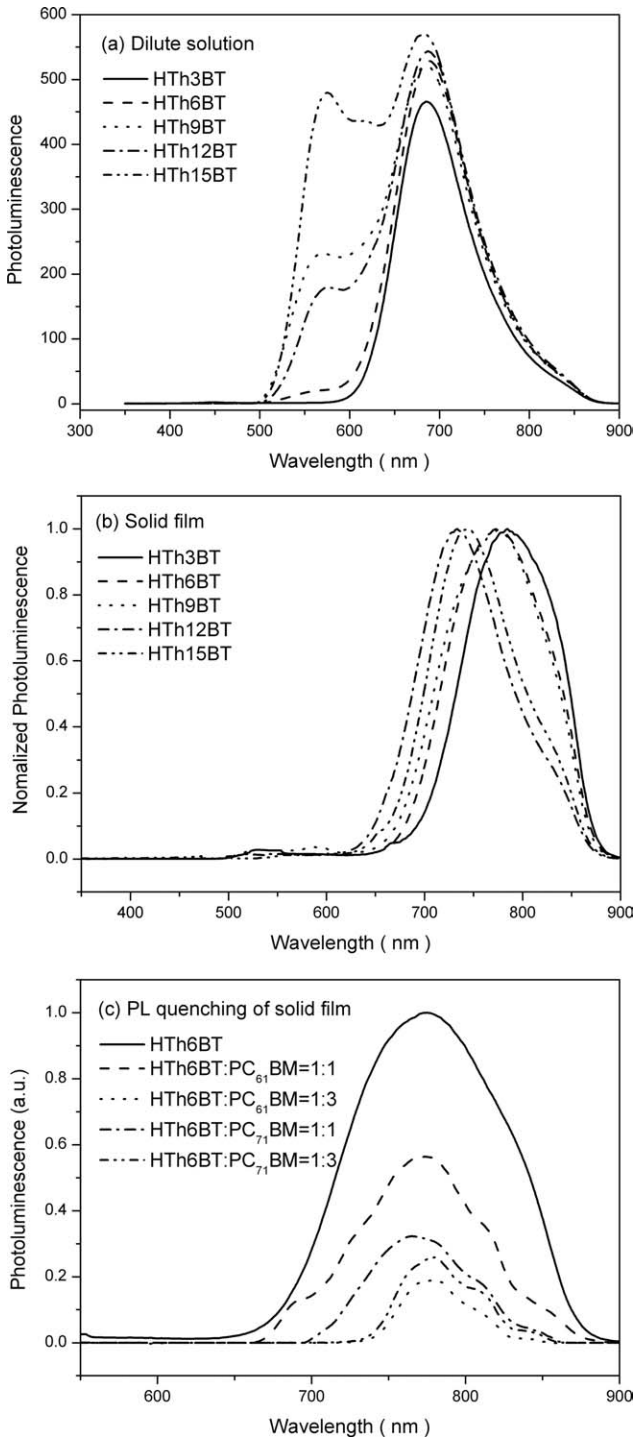

FIGURE 3 Comparison of PL spectra of polymers (a) in a solution (in chloroform at a concentration of 1 mg/mL), and (b) in a film, and (c) PL quenching for HTh6BT/PCBM blend films.

the red emission region with a maximum emission near 800 nm.

On the basis of all these optical measurements, HTh6BT was the best active material for the OPVs. The PL spectra of the HTh6BT/PCBM blend films were measured prior to the photovoltaic device fabrication to investigate the quenching ratio of the excitons. In Figure 3(c), the generated excitons were efficiently quenched in the HTh6BT/$PC_{71}BM$ (1:3, w/w) blend system. The fast photo-induced charge carriers were efficiently transferred from the donor to the acceptor in the system, and therefore, the best photovoltaic properties were observed at these conditions. The maximum wavelengths of the absorption peaks and the optical bandgaps of the polymers are summarized in Table 2.

Electrochemical Properties

The electrochemical behavior of the copolymers was investigated using cyclic voltammetry (CV). The supporting electrolyte was tetrabutyl ammonium hexafluorophosphate (Bu_4NPF_6) in acetonitrile (0.1 M), and the scan rate was 50 mV/s. The ITO glass and Pt plates were used as the working and counter electrodes, respectively, and silver/silver chloride (Ag in 0.1 M KCl) was used as the reference electrode. All of other measurements were calibrated using the ferrocene value of −4.8 eV as the standard. The HOMO levels of the polymers were determined using the oxidation onset value. The LUMO levels were calculated from the differences between the HOMO energy levels and the optical band-gaps, which was determined using the UV–vis absorption onset value in the films.

Figure 4 shows the cyclic voltammograms of the synthesized polymers. According to these results, the HOMO levels of synthesized polymers were −5.08 to −5.24 eV, and the LUMO levels were –3.46 to –3.52 eV. In Table 2, except for HTh6BT, the HOMO energy levels decreased and the bandgap increased with increasing molar ratio of 3-hexylthiophene in the polymer backbone. Since HTh3BT had the strongest ICT effect between electron donating unit (alkylthiophene) and electron withdrawing unit (benzothiadiazole) of all these polymer, it shows high HOMO energy level. The HOMO energy level decreased with increase of 3-hexylthiophene ratios in other polymers due to decrease of ICT effect. However, HTh6BT showed a sharp drop of the HOMO energy level, it relies on effective interaction between intrachain molecules as well as decrease of ICT effect. From these results, HTh6BT, among the five polymers, likely had an effective π-conjugation length for obtaining a well balanced energy level and an intermolecular interaction. Considering the well-balanced energy level and the low bandgap of HTh6BT, HTh6BT was expected to exhibit the best power conversion efficiency of the five polymers. The electrochemical properties of the polymers are summarized in Table 2.

XRD Analysis

In Figure 5, the X-ray diffraction (XRD) measurements were carried out on the polymer powders to determine the microstructure of the synthesized polymers. All of the polymers exhibited short π-π stacking distances (d_2 = 3.8–4.0 Å). This d_2 value corresponded to the distance between the coplanar π-conjugated main chains and was an important factor in determining the intermolecular interaction. Since all five polymers were based on 3-hexylthiophene, the π-π stacking distances of these polymers were similar to P3HT (d_2 = 3.8 Å). However, very weak π-π stacking peak intensities were

TABLE 2 Optical, Electrochemical Data, and Energy Levels of HThmBT Series

	Absorption λ_{max} (nm)[a]		PL λ_{max} (nm)[b]				Energy Level[e] (eV)	
Polymer	Solution[f]	Film[g]	Solution[f]	Film[g]	$E_g^{op,c}$ (eV)	$E_{onset}^{ox,d}$	HOMO	LUMO
HTh3BT	387,553	421,609	686	785	1.6	0.75	−5.08	−3.48
HTh6BT	408,536	408,596	688	775	1.65	0.89	−5.22	−3.57
HTh9BT	414,521	454	570,686	777	1.67	0.82	−5.15	−3.48
HTh12BT	426	442	576,687	733	1.72	0.85	−5.18	−3.46
HTh15BT	428	491	576,683	746	1.72	0.91	−5.24	−3.52

[a] λ_{max} was determined from UV-vis data.
[b] λ_{max} was determined from PL data.
[c] Estimated from the onset of UV–vis absorption data of the thin film.
[d] Onset oxidation potential.
[e] Calculated from the reduction and oxidation potentials under the assumption that the absolute energy level of Fc/Fc+ was 4.8 eV below a vacuum.
[f] Diluted in chloroform.
[g] Spin-coated from a chloroform.

observed for the polymers, except for HTh6BT. HTh3BT showed low degree of crystallinity since HTh3BT had not only short repeating units of 3-hexylthiophene but also structural irregularity. A degree of crystallinity was supposed to be increased with increase of 3-hexylthiophene ratios in other polymers due to characteristics of P3HT moiety that had high degree of crystallinity. These polymers appeared to have a weak intermolecular interaction and low crystallinity, which led to low carrier mobility and low current density properties in the photovoltaic device. In contrast to the other four polymers, HTh6BT exhibited a high diffraction intensity and a short π-π stacking distance (d_2 = 3.9 Å). HTh6BT had higher structural regularity than HTh3BT and other polymers, and it was likely to come from effective intermolecular and intramoleular interaction. Considering the optical, electrochemical, and structural measurement results, HTh6BT exhibited better electronic properties than the other polymers in the photovoltaic device.

Photovoltaic Properties

All of the synthesized polymers were applied in the bulk heterojunction geometry (BHG) with PCBM. The OPV cells were fabricated with the sandwiched glass/ITO/PEDOT:PSS/polymer-PCBM (1:3, w:w)/BaF_2/Ba/Al structure. A blend of the polymer (7.5 mg/mL of the polymer in CB) and $PC_{71}BM$ was dissolved in CB, filtered through a 0.45-μm poly(tetrafluoroethylene) (PTFE) filter, and spin coated at 500–1100 rpm for 30 s. The active layers were preannealed at 120 °C for 10 min before the electrode deposition. Each substrate was patterned using photolithography techniques to produce a segment with an active area of 9.0 mm^2. After all of the fabricated devices were encapsulated in a glove box, the I-V characteristics were measured under an ambient atmosphere.

Figure 6 illustrates the I-V properties of the fabricated devices. $PC_{61}BM$ and $PC_{71}BM$ were introduced as acceptor materials to confirm the acceptor effect in the polymer/PCBM blend. HTh3BT–HTh15BT exhibited V_{OC} values of 0.7–0.82 V and J_{SC} values of 1.3–3.4 mA/cm^2 when $PC_{61}BM$ was used as the acceptor. On the other hand, when $PC_{71}BM$ was used, the V_{OC} values were similar to the V_{OC} values that were measured when $PC_{61}BM$ was used as the acceptor, but the J_{SC} values of the synthesized polymers obviously increased to

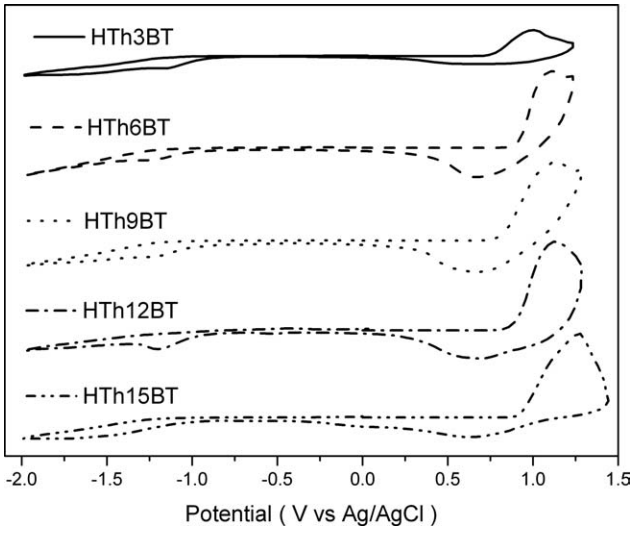

FIGURE 4 Cyclic voltammograms of thin films recorded in 0.1 M Bu_4NPF_6/acetonitrile at a scan rate of 50 mV/s.

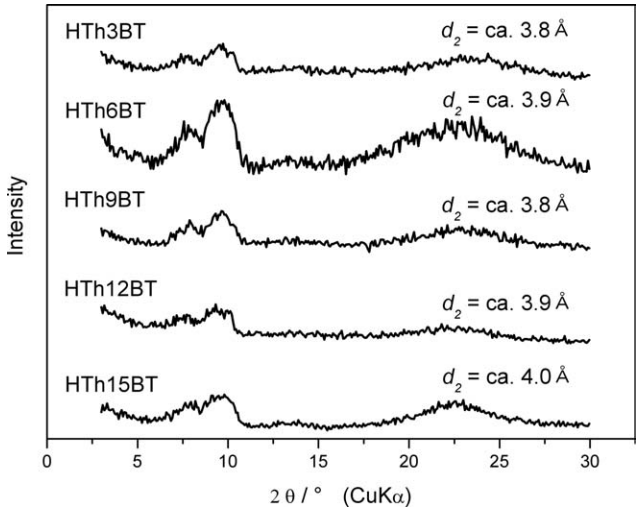

FIGURE 5 X-ray diffraction patterns of powdery HThmBT series.

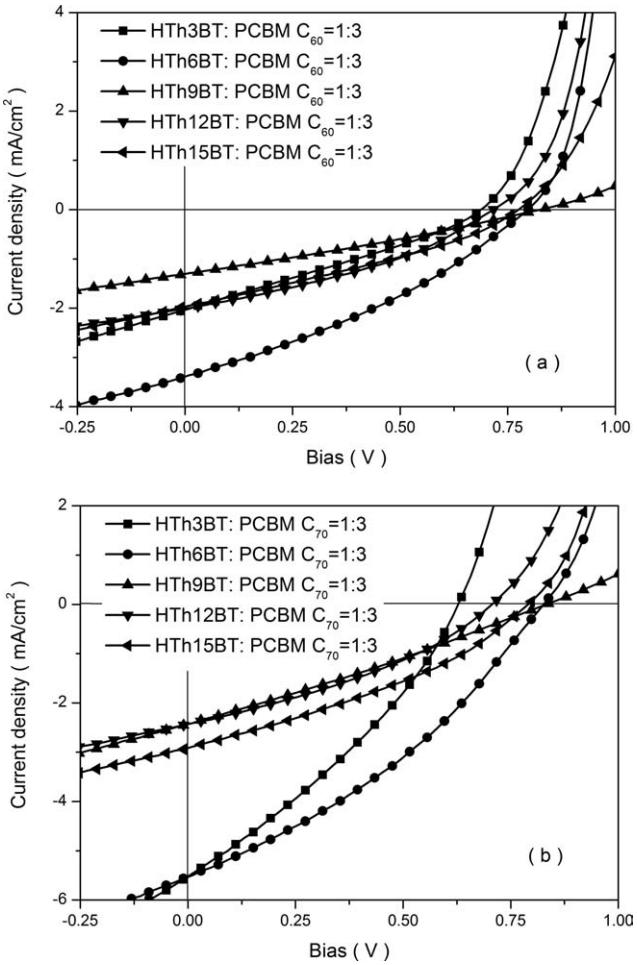

FIGURE 6 I-V characteristics of photovoltaic devices (polymer:PCBM = 1:3) that have (a) HThmBT/$PC_{61}BM$, and (b) HThmBT/$PC_{71}BM$ blend films as active layers.

values from 2.4 to 5.5 mA/cm^2. As expected, the best performance data were obtained in the device that used the HTh6BT/$PC_{71}BM$ blend film as the active layer, corresponding to a V_{OC} of 0.82 V, a J_{SC} of 5.5 mA/cm^2, a FF of 0.34, and a PCE of 1.6%. HTh3BT and HTh6BT exhibited higher PCE values than HTh9BT to HTh15BT because they exhibited better photon absorption properties in the long wavelength range. Although HTH6BT had a narrow overlapping range in the solar spectrum with respect to HTh3BT, HTh6BT had a higher PCE value than HTh3BT because the high structural regularity led to similar current density values to HTh3BT. Furthermore, HTh6BT had a high V_{OC} value of 0.82 V. A variety of polymers based on alkylthiophene and benzothiadiazole were investigated in the previous literature, but they exhibited low V_{OC} values of ~0.6 V.[43,44] In comparison to these polymers, the HThmBT polymer series that was synthesized in this study exhibited high V_{OC} values of 0.7–0.84 V. Considering that V_{OC} depends on recombination process of generated excitons and the HOMO energy level of donor polymer, it is likely that high V_{OC} values of HThmBT come from low HOMO energy level of those and improved planarity of polymer backbone. HThmBT has lower HOMO energy level than other alkylthiophene- and benzothiadiazole-based polymers. Moreover, planar backbone structure of regioregular head to tail type alkylthiophene moieties increases lifetime of excitons, which decrease recombination ratio of excitons.

In contrast, the low PCE value of HTh9BT originated from the reduced ICT effect and the structural irregularity. The ICT effect decreased with increasing 3-hexylthiophene molar ratio. Moreover, the length of the repeating units of the 3-hexylthiophene oligomers was not long enough to improve the structural regularity. HTh12BT and HTh15BT exhibited better PCE values than HTh9BT because of their higher 3-hexylthiophene molar ratios compared to HTh9BT. The better performance of these devices could have originated from improvement in the structural regularity, which resulted in the improvement of the intermolecular interaction.

The external quantum efficiency (EQE) measurements were carried out to investigate the origin of the differences in the current density. The good current density properties of HTh3BT and HTh6BT were compared to the bad current density properties of HTh9BT. In Figure 7, the HTh3BT/$PC_{71}BM$ and HTh6BT/$PC_{71}BM$ films exhibited EQE values of 23 and 18%, respectively, at 400–450 nm. In contrast to these two polymers, HTh9BT exhibited an EQE value of 6% in the same absorption range. Although HTh6BT had a lower EQE value than HTh3BT, the two polymers had the same photocurrent density of 5.5 mA/cm^2, which likely originated from the improved intermolecular interaction of HTh6BT that depended on the structural regularity. Taking all of these results into account, the current density of the five polymers influenced the optical properties and the nature of the intermolecular structure. The photovoltaic properties of the polymers are summarized in Table 3.

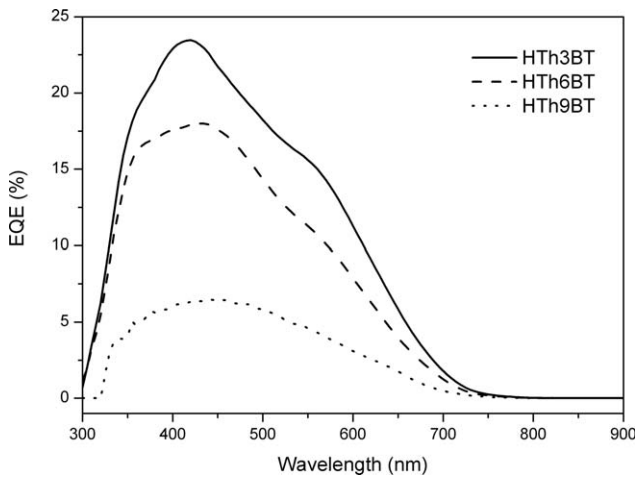

FIGURE 7 EQE spectra of photovoltaic devices that have HTh3BT, HTh6BT (polymers that have a good current density), and HTh9BT (polymer that has a bad current density) as a donor materials, respectively, and $PC_{71}BM$ as an acceptor.

TABLE 3 Photovoltaic Characteristics of Devices that have HThmBT/PCBM Blend Films as Active Layers

Polymer	Jsc[a] (mA/cm^2)	Voc[a] (V)	FF[a]	η[a] (%)
HTh3BT[b]	2.0	0.70	28.5	0.40
HTh6BT[b]	3.4	0.80	32.0	0.88
HTh9BT[b]	1.3	0.82	28.8	0.30
HTh12BT[b]	2.0	0.72	35.2	0.50
HTh15BT[b]	2.0	0.78	31.9	0.48
HTh3BT[c]	5.5	0.64	32.0	1.10
HTh6BT[c]	5.5	0.82	34.6	1.60
HTh9BT[c]	2.4	0.84	27.7	0.55
HTh12BT[c]	2.4	0.70	35.2	0.59
HTh15BT[c]	2.9	0.80	33.8	0.78

[a] Under AM 1.5 simulated solar illumination at an irradiation intensity of 100 mW/cm^2.
[b] Using a $PC_{61}BM$ as a acceptor (polymer:$PC_{61}BM$ = 1:3, w/w).
[c] Using a $PC_{71}BM$ as a acceptor (polymer:$PC_{71}BM$ = 1:3, w/w).

EXPERIMENTAL

Instruments and Characterization

All of the reagents and chemicals were purchased from Aldrich and used as received unless otherwise specified. The ^{1}H-NMR (400 MHz) spectra were recorded using a Brüker AMX400 spectrometer in $CDCl_3$, and the chemical shifts were recorded in units of ppm with TMS as the internal standard. The elemental analyses were measured with EA1112 using a CE Instrument. The absorption spectra were recorded using an Agilent 8453 UV-visible spectroscopy system. The PL spectra were measured using a Hitachi F-4500 spectrophotometer. The solutions that were used for the UV–visible spectroscopy, and photoluminescence (PL) efficiency measurements were dissolved in chloroform at a concentration of 1 mg/mL. The films were drop-coated from the chloroform solution onto a quartz substrate. All of the GPC analyses were carried out using THF as the eluent and a polystyrene standard as the reference. The TGA measurements were performed using a TA Instrument 2050. The cyclic voltammetric waves were produced using a Zahner IM6eX electrochemical workstation with a 0.1-M acetonitrile (substituted with nitrogen in 20 min) solution containing Bu_4NPF_6 as the electrolyte at a constant scan rate of 50 mV/s. ITO, a Pt wire and silver/silver chloride (Ag in 0.1 M KCl) were used as the working, counter, and reference electrodes, respectively. The electrochemical potential was calibrated against Fc/Fc^+. The current-voltage (I-V) curves of the photovoltaic devices were measured using a computer-controlled Keithley 2400 source measurement unit (SMU) that was equipped with a Peccell solar simulator under an illumination of AM 1.5G (100 mW/cm^2). The X-ray diffraction (D/Max-2200, Rigaku Denki) patterns were obtained at 40 kV and 30 mA using Cu Kα radiation with a characteristic wavelength of 0.154 nm in a 2θ range of 1–50° at a scanning rate of 4°/min.

Fabrication and Characterization of Polymer Solar Cells

All of the bulk-heterojunction PV cells were prepared using the following device fabrication procedure. The glass/indium tin oxide(ITO) substrates [Sanyo, Japan (10 Ω/γ)] were sequentially lithographically patterned, cleaned with detergent, and ultrasonicated in deionized water, acetone, and isopropyl alcohol. Then the substrates were dried on a hotplate at 120 °C for 10 min and treated with oxygen plasma for 10 min to improve the contact angle just before the film coating process. Poly(3,4-ethylene-dioxythiophene):poly(styrene-sulfonate) (PEDOT:PSS, Baytron P 4083 Bayer AG) was passed through a 0.45-μm filter before being deposited onto ITO at a thickness of about 32 nm through spin-coating at 4000 rpm in air and then dried at 120 °C for 20 min inside a glove box. A mixture of the polymers/PCBM [1:1 (w/w)/1:3 (w/w)], 7.5 mg/mL in chlorobenzene was stirred over night, filtered through a 0.45-μm PTFE filter, and then spin-coated (500–1100 rpm, 30 s) on top of the PEDOT:PSS layer. The device fabrication was completed by depositing thin layers of BaF_2 (1 nm), Ba (2 nm), and Al (200 nm) at pressures less than 10^{-6} torr. The active area of the device was 9.0 mm^2. Finally, the cell was encapsulated using UV-curing glue (Nagase, Japan). The illumination intensity was calibrated using a standard Si photodiode detector that was equipped with a KG-5filter. The output photocurrent was adjusted to match the photocurrent of the Si reference cell to obtain a power density of 100 mW/cm^2. After the encapsulation, all of the devices were operated under an ambient atmosphere at 25 °C.

SYNTHESIS

Synthesis of 2,5-Bis(trimethyl stannyl)thiophene (1)

2,5-Dibromothiophene (2.75 g, 11.36 mmol) was dissolved in THF (45.4 mL), and the solution was cooled to −50 °C. Then a 2.5 M solution of *n*-BuLi in hexane (10 mL, 25 mmol) was added dropwise for 1 h, and the resulting mixture was stirred for 30 min at −50 °C. After 30 min, the solution was cooled again to −78 °C, and a 1.0-M solution of Me_3SnCl in THF (25 mL, 25 mmol) was added for 1 h. After stirring at −78 °C for 3 h, the solution was allowed to warm up to room temperature and was stirred 24 h. Then this mixture was poured into *n*-hexane, washed with $NaHCO_3$ and water twice, and the dried over Na_2SO_4. The solvents were removed through rotary evaporation to afford a brown solid. The crude product was recrystallized with hexane to produce the light-brown crystals (2.79 g, 60%). ^{1}H-NMR (400 MHz, $CDCl_3$, ppm): δ 0.36 (t, J = 27.4 Hz, 18H), 7.37 (s, 2H)

Synthesis of 4,7-Dibromobenzothiadiazole (2)

2,1,3-Benzothiadiazole (10.00 g, 73.44 mmol) and 150 mL of HBr were added to a 500-mL two-necked round bottom flask. A solution containing Br_2 (35.21 g, 220.32 mmol) in 100 mL of HBr was very slowly added dropwise (the slow addition was essential). If necessary, an additional 100 mL of HBr was added to the solution. After the total addition of Br_2, the solution was refluxed for 6 h, and an orange solid was precipitated. The mixture was allowed to cool to room temperature, and a sufficiently saturated solution of $NaHSO_3$ was added to completely consume any excess Br_2. The mixture was filtered under vacuum and exhaustively washed with water. The solid was then washed once with cold Et_2O and dried under vacuum for 20 h. The yellow crude product

was recrystallized with chloroform to afford the desired product at an 85% yield (17.3 g). ^{1}H-NMR (400 MHz, $CDCl_3$, ppm): δ 7.73 (s, 2H). ^{13}C-NMR (100 MHz, $CDCl_3$, ppm): 153.34, 132.67, 114.31.

Synthesis of 2-Bromo-3-hexylthiophene (3)

First, 51.7 mL of acetic acid and 51.7 mL of $CHCl_3$ were added to a dry round bottom flask, and the flask was purged with nitrogen for 10 min. Then 3-hexylthiophene (8.7 g, 51.7 mmol) was added. The mixture was cooled to 5 °C, and NBS (9.2 g, 51.7 mmol) was added over a period of 1 h while the temperature was maintained at 5−10 °C. The mixture was stirred overnight and cooled in an ice bath. Then a dilute HCl solution (100 mL) was added, and the mixture was extracted with $CHCl_3$. The $CHCl_3$ layer was washed with water several times until a pH 6 was reached, and then this layer was dried over anhydrous Na_2SO_4. The solvent was removed through rotary evaporation. The residue was chromatographed on a silica gel using hexane as the eluent. After flash chromatography, the yield of the final compound was 92% (11.82 g, colorless liquid). ^{1}H-NMR (400 MHz, $CDCl_3$, ppm): δ 0.88 (t, J = 6.4 Hz, 3H), 1.34 (m, 6H), 1.57 (t, J = 7.0 Hz, 3H), 2.53 (t, J = 7.7 Hz, 2H), 6.78 (d, J = 5.6 Hz, 1H), 7.18 (d, J = 5.6 Hz, 1H)

Synthesis of 2-Bromo-3-hexyl-5-trimethylstannylthiophene (4)

2-Bromo-3-hexylthiophene (12 g, 50 mmol) was dissolved in THF (41 mL), and the solution was cooled to −78 °C. Then a 2.0-M solution of lithium diisopropylamine in THF (28 mL, 56 mmol) was added dropwise for 1 h. After stirring for 1 h at −78 °C, a 1.0-M solution of Me_3SnCl in THF (56 mL, 56 mmol) was added dropwise, and the mixture was stirred at −50 °C for 2 h. Then the solution was allowed to warm up to room temperature and was stirred 24 h. After the reaction was completed, the reaction mixture was poured into water and extracted with ether. The organic phase was washed with brine several times and dried over Na_2SO_4. The solvents were removed through rotary evaporation to afford a brown liquid. The residue was reduced-distilled to produce a 76% yield (15.6 g) of the product as a colorless oil. ^{1}H-NMR (400 MHz, $CDCl_3$, ppm): δ 0.36 (t, J = 27.6 Hz, 9H), 0.88 (t, J = 6.8 Hz, 3H), 1.31 (m, 6H), 1.56 (t, J = 7.2 Hz, 2H), 2.55 (t, J = 7.6 Hz, 2H), 6.85 (s, 1H). ^{13}C-NMR (400 MHz, DMSO-d_6, ppm): −7.56 (m), 14.75, 23.28, 29.73, 29.95, 30.54, 32.31, 114.12, 136.97 (m), 138.62, 143.80.

GENERAL PROCEDURE OF POLYMERIZATION THROUGH THE STILLE REACTION

Equimolar amounts (0.4 mmol) of 2,5-bis(trimethyl stannyl)thiophene and 4,7-dibromo-2,1,3-benzothiadiazole were dissolved in DMF (0.125*M*). After mild heating for 1 h, different amounts of 2-bromo-3-hexyl-5-trimethylstannylthiophene (P1: 1.2 mmol, P2: 2.4 mmol, P3: 3.6 mmol, P4: 4.8 mmol, and P5: 6.0 mmol) were added. Then 1.25 mol % of $Pd(PPh_3)_2Cl_2$ was added to the mixture. The orange solution was warmed to 120 °C and allowed to reflux for 48 h under N_2. 2-Bromo thiophene was systematically added to the end-cap of the polymer chain. After cooling to room temperature, the polymer was poured into methanol (300 mL) and filtered. The filtered polymer was further dissolved in $CHCl_3$, reprecipitated into methanol, and filtered again. The polymer was further purified through washing with methanol, acetone, and hexane in a Soxhlet apparatus for 24 h. The chloroform soluble fraction was recovered and dried under a reduced pressure at 50 °C.

HTh3BT

Black solid 0.294 g (yield = 84%). ^{1}H-NMR ($CDCl_3$, ppm): δ 0.925 (s, 9H), 1.26−1.71 (m, 22H), 2.62−2.82 (m, 6H), 7.08 (s, 3H), 7.83−7.98 (d, 4H). Anal. calcd for C_{40} H_{43} N_2 S_5: C, 67.69; H, 7.03; N, 3.76; S, 21.51. Found: C, 65.42; H, 6.37; N, 4.01; S, 21.71.

HTh6BT

Black solid 0.369 g (yield = 84%). ^{1}H-NMR ($CDCl_3$, ppm): δ 0.912 (s, 16H), 1.25−1.71 (m, 48H), 2.58 (s, 2H), 2.80 (d, 9H), 6.98−7.09 (d, 6H), 7.83−7.98 (d, 4H). Anal. calcd for C_{70} H_{88} N_2 S_8: C, 69.51; H, 7.62; N, 2.25; S, 20.62. Found: C, 68.47; H, 7.39; N, 2.38; S, 20.75.

HTh9BT

Black solid 0.535 g (yield = 87%). ^{1}H-NMR ($CDCl_3$, ppm): δ 0.913 (s, 27H), 1.25−1.71 (m, 70H), 2.59 (s, 2H), 2.80 (d, 15H), 6.98−7.09 (d, 9H), 7.83−7.98 (d, 4H). Anal. calcd for C_{100} H_{130} N_2 S_{11}: C, 70.29; H, 7.87; N, 1.61; S, 20.24. Found: C, 69.01; H, 7.84; N, 1.71; S, 19.96.

HTh12BT

Black solid 0.745 g (yield = 94%). ^{1}H-NMR ($CDCl_3$, ppm): δ 0.914 (s, 38H), 1.25−1.77 (m, 98H), 2.57 (s, 4H), 2.80 (d, 20H), 6.98−7.11 (d, 14H), 7.83−7.98 (d, 4H). Anal. calcd for C_{130} H_{172} N_2 S_{14}: C, 70.72; H, 8.00; N, 1.25; S, 20.02. Found: C, 70.68; H, 7.97; N, 1.31; S, 20.05.

HTh15BT

Black solid 0.713 g (yield = 98%). ^{1}H-NMR ($CDCl_3$, ppm): δ 0.914 (s, 54H), 1.25−1.71 (m, 124H), 2.57 (s, 6H), 2.80 (d, 28H), 6.98−7.14 (d, 18H), 7.84−7.99 (d, 4H). Anal. calcd for C_{160} H_{214} N_2 S_{17}: C, 71.00; H, 8.09; N, 1.02; S, 19.89. Found: C, 70.81; H, 8.12; N, 0.98; S, 19.72.

CONCLUSIONS

In summary, five DA-type copolymers, based on 3-hexylthiophene and 2,1,3-benzothiadiazole, were successfully synthesized through the Stille coupling reaction for the OPVs. These copolymers exhibited low bandgaps of 1.6−1.72 V and high open circuit voltages of 0.7−0.84 V. HTh6BT exhibited a well-balanced energy level and a good PCE value of 1.6% (V_{OC} = 0.82 V, J_{SC} = 5.5 mA/cm^2, FF = 0.35) because of the absorption properties in the long range of the solar spectrum, the low LUMO energy level, and the structural regularity of HTh6BT over the other polymers in photovoltaic device. In particular, the polymers had high V_{OC} values despite being based on thiophene. Additives, such as 1, 8-octanedithiol and 1,8-diiodooctane, on the fabricating active layer could be used to increase the J_{SC} and FF values because HTh6BT exhibited good intrinsic properties.

This work was supported by the National Research Foundation of Korea Grant funded by the Korean Government(MEST) (NRF-2009-C1AAA001-2009-0093526).

REFERENCES AND NOTES

1 Chen, G. Y.; Chiang, C. M.; Kekuda, D.; Lan, S. C.; Chu, C. W.; Wei, K. H. J Polym Sci Part A: Polym Chem 2010, 48, 1669–1675.

2 Chen, H. Y.; Hou, J.; Hayden, A. E.; Yang, H.; Houk, K. N.; Yang, Y. Adv Mater 2010, 22, 371–375.

3 Jung, I. H.; Kim, H.; Park, M. J.; Kim, B.; Park, J. H.; Jeong, E.; Woo, H. Y.; Yoo, S. H.; Shim, H. K. J Polym Sci Part A: Polym Chem 2010, 48, 1423–1432.

4 Helgesen, M.; Søndergaard, R.; Krebs, F. C. J Mater Chem 2010, 20, 36–60.

5 Krebs, F. C. Sol Energy Mater Sol Cells 2009, 93, 394–412.

6 Kippelen, B.; Brédas, J. Energy Environ Sci 2009, 2, 251–261.

7 Lee, J. Y.; Heo, S. W.; Choi, H.; Kwon, Y. J.; Haw, J. R.; Moon, D. K. Sol Energy Mater Sol Cells 2009, 93, 1932–1938.

8 Soci, C.; Hwang, I. W.; Moses, D.; Zhu, Z.; Waller, D.; Gaudiana, R.; Brabec, C. J.; Heeger, A. J. Adv Funct Mater 2007, 17, 632–636.

9 Kim, D. H.; Lee, B. L.; Moon, H.; Kang, H. M.; Jeong, E. J.; Park, J. I.; Han, K. M.; Lee, S.; Yoo, B. W.; Koo, B. W.; Kim, J. Y.; Lee, W H.; Cho, K.; Becerril, H. A.; Bao, Z. J Am Chem Soc 2009, 131, 6124–6132.

10 Allard, S.; Forster, M.; Souharce, B.; Thiem, H.; Scherf, U. Angew Chem Int Ed 2008, 47, 4070–4098.

11 Zhang, M.; Tsao, H. N.; Pisula, W.; Yang, C.; Mishra, A. K.; Müllen, K. J Am Chem Soc 2007, 129, 3472–3473.

12 Song, K. W.; Lee, J. Y.; Heo, S. W.; Moon, D. K. J Nanosci Nanotech 2010, 10, 99–105.

13 Kim, S. O.; Jung, H. C.; Lee, M. J.; Jun, C.; Kim, Y. H.; Kwon, S. K. J Polym Sci Part A: Polym Chem 2009, 47, 5908–5916.

14 Liu, J.; Cheng, Y.; Xie, Z.; Geng, Y.; Wang, L.; Jing, X.; Wang, F. Adv Mater 2008, 20, 1357–1362.

15 Lee, J. Y.; Kwon, Y. J.; Woo, J. W.; Moon, D. K. J Ind Eng Chem 2008, 14, 810–817.

16 Oh, S. Y.; Lee, C. H.; Ryu, S. H.; Oh, H. S. J Ind Eng Chem 2006, 12, 69–75.

17 Krebs, F. C. Sol Energy Mater Sol Cells 2009, 93, 465–475.

18 Krebs, F. C.; Gevorgyan, S. A.; Alstrup, J. J Mater Chem 2009, 19, 5442–5451.

19 Krebs, F. C. Org Electron 2009, 10, 761–768.

20 Krebs, F. C.; Gevorgyan, S. A.; Gholamkhass, B.; Holdcroft, S.; Schlenker, C.; Thompson, M. E.; Thompson, B. C.; Olson, D.; Ginley, D. S.; Shaheen, S. E.; Alshareef, H. N.; Murphy, J. W.; Youngblood, W. J.; Heston, N. C.; Reynolds, J. R.; Jia, S.; Laird, D.; Tuladhar, S. M.; Dane, J. G. A.; Atienzar, P.; Nelson, J.; Kroon, J. M.; Wienk, M. M.; Janssen, R. A. J.; Tvingstedt, K.; Zhang, F.; Andersson, M.; Inganäs, O.; Lira-Cantu, M.; de Bettignies, R.; Guillerez, S.; Aernouts, T.; Cheyns, D.; Lutsen, L.; Zimmermann, B.; Würfel, U.; Niggemann, M.; Schleiermacher, H.; Liska, P.; Grätzel, M.; Lianos, P.; Katz, E. A.; Lohwasser, W.; Jannon, B. Sol Energy Mater Sol Cells 2009, 93, 1968–1977.

21 Tipnis, R.; Bernkopf, J.; Jia, S.; Krieg, J.; Li, S.; Storch, M.; Laird, D. Sol Energy Mater Sol Cells 2009, 93, 442–446.

22 Niggemann, M.; Zimmermann, B.; Haschke, J.; Glatthaar, M.; Gombert, A. Thin Solid Films 2008, 516, 7181–7187.

23 Park, S. H.; Roy, A.; Beaupré, S.; Cho, S.; Coates, N.; Moon, J. S.; Moses, D.; Leclerc, M.; Lee, K.; Heeger, A. J. Nature Photonics 2009, 3, 297–303.

24 Blouin, N.; Michaud, A.; Gendron, D.; Wakim, S.; Blair, E.; Neagu-Plesu, R.; Belletête, M.; Durocher, G.; Tao, Y.; Leclerc, M. J Am Chem Soc 2008, 130, 732–742.

25 Mühlbacher, D.; Scharber, M.; Morana, M.; Zhu, Z.; Waller, D.; Gaudiana, R.; Brabec, C. Adv Mater 2006, 18, 2884–2889.

26 Li, G.; Shrotriya, V.; Huang, J. S.; Yao, Y.; Moriarty, T.; Emery, K.; Yang, Y. Nature Mater 2005, 4, 864–868.

27 Reyes-Reyes, M.; Kim, K.; Dewald, J.; López-Sandoval, R.; Avadhanula, A.; Curran, S.; Carroll, D. L. Org Lett 2005, 7, 5749–5752.

28 Reyes-Reyes, M.; Kim, K.; Carroll, D. L. Appl Phys Lett 2005, 87, 083506.

29 Kim, J. Y.; Lee, K.; Coates, N. E.; Moses, D.; Nguyen, T.; Dante, M.; Heeger, A. J. Science 2007, 317, 222–225.

30 Bundgaard, E.; Krebs, F. C. Sol Energy Mater Sol Cells 2007, 91, 954–985.

31 Scharber, M. C.; Mühlbacher, D.; Koppe, M.; Denk, P.; Waldauf, C.; Heeger, A. J.; Brabec, C. J. Adv Mater 2006, 18, 789–794.

32 Cheng, Y. J.; Yang, S. H.; Hsu, C. S. Chem Rev 2009, 109, 5868–5923.

33 Lee, J. Y.; Shin, W. S.; Haw, J. R.; Moon, D. K. J Mater Chem 2009, 19, 4938–4945.

34 Gadisa, A.; Mammo, W.; Andersson, L. M.; Admassie, S.; Zhang, F.; Andersson, M. R.; Inganäs, O. Adv Funct Mater 2007, 17, 3836–3842.

35 Bundgaard, E.; Shaheen, S. E.; Krebs, F. C.; Ginley, D. S. Sol Energy Mater Sol Cells 2007, 91, 1631–1637.

36 Newman, C. R.; Frisbie, C. D.; da Silva Filho, D. A.; Brédas, J. L.; Ewbank, P. C.; Mann, K. R. Chem Mater 2004, 16, 4436–4451.

37 Ong, B. S.; Wu, Y.; Liu, P.; Gardner, S. J Am Chem Soc 2004, 126, 3378–3379.

38 Hwang, I. W.; Xu, Q. H.; Soci, C.; Chen, B.; Jen, A. K. Y.; Moses, D.; Heeger, A. J. Adv Funct Mater 2007, 17, 563–568.

39 Jestin, I.; Frère, P.; Mercier, N.; Levillain, E.; Stievenard, D.; Roncali, J. J Am Chem Soc 1998, 120, 8150–8158.

40 Elandaloussi, E. H.; Frère, P.; Richomme, P.; Orduna, J.; Garin, J.; Roncali, J. J Am Chem Soc 1997, 119, 10774–10784.

41 Yasuda, T.; Imase, T.; Yamamoto, T. Macromolecules 2005, 38, 7378–7385.

42 Yamamoto, T.; Lee, B. L.; Kokubo, H.; Kishida, H.; Hirota, K.; Wakabayashi, T.; Okamoto, H. Macromol Rapid Commun 2003, 24, 440–443.

43 Bundgaard, E.; Krebs, F. C. Macromolecules 2006, 39, 2823–2831.

44 Bundgaard, E.; Krebs, F. C. Polym Bull 2005, 55, 157–164.